

# The influence of structure geometry and material on seismic metamaterial performance

T. Venkatesh Varma<sup>1</sup>, Bogdan Ungureanu<sup>2</sup>, Saikat Sarkar<sup>1</sup>, Richard Craster<sup>2,3,4</sup>,  
Sébastien Guenneau<sup>4</sup>, Stéphane Brûlé<sup>5</sup>

<sup>1,\*</sup>Discipline of Civil Engineering, Indian Institute of Technology, Indore, India

<sup>2</sup>Department of Mathematics, Imperial College London, London SW7 2AZ,  
United Kingdom

<sup>3</sup>Department of Mechanical Engineering, Imperial College London, London SW7  
2AZ, United Kingdom

<sup>4</sup>UMI 2004 Abraham de Moivre-CNRS, Imperial College London, London SW7  
2AZ, United Kingdom

<sup>5</sup>Aix Marseille Univ, CNRS, Centrale Marseille, Institut Fresnel, France

\*Corresponding Author, E-mail: b.ungureanu@imperial.ac.uk

## Abstract

Diverting, and controlling, elastic vibrations impacting upon infrastructure is a major challenge for seismic hazard mitigation, and for the reduction of machine noise and vehicle vibration in the urban environment. Seismic metamaterials (SMs), with their inherent ability to manipulate wave propagation, provide a key route for overcoming the technological hurdles involved in this challenge. Engineering the structure of the SM serves as a basis to tune and enhance its functionality, and inspired by split rings, swiss-rolls, notch-shaped and labyrinthine designs of elementary cells in electromagnetic and mechanical metamaterials, we investigate altering the structure geometries of SMs with the aim of creating large bandgaps in a subwavelength regime. We show that square stiff inclusions, perform better in comparison to circular ones, whilst keeping the same filling fraction. En route to enhancing the bandgap, we have also studied the performance of SMs with different constituent materials; we find that steel columns, as inclusions, show large bandgaps, however, the columns are too large for steel to be a feasible material in practical or financial terms. Non-reinforced concrete would be preferable for industry level scaling up of the technology because, concrete is cost-effective, easy to cast directly

at the construction site and easy to provide arbitrary geometry of the structure. As a part of this study, we show that concrete columns can also be designed to exhibit bandgaps if we cast them within a soft soil coating surrounding the protected area for various civil structures like a bridge, building, oil pipelines etc. Although our motivation is for ground vibration, and we use the frequencies, lengthscales and material properties relevant for that application, it is notable that we use the equations of linear elasticity and our investigation is more broadly relevant in solid mechanics.

## 1 Introduction

Controlling elastic waves near structures is key to addressing a large class of civil engineering problems ranging from seismic hazard mitigation to stopping unwanted noise and vibration produced by vehicles, heavy machinery on construction sites etc. [1, 2, 3, 4]. Seismic waves lead to the destruction of civil installations and loss of life, thus forming one of the most important and difficult challenges for civil engineers; the reduction of urban noise and vibration is also important because they create health issues and have other consequences such as affecting highly sensitive scientific and medical instruments. There are many other applications, e.g., in the context of ground motions produced from even minor tremors, industrial machinery or suburban rail transport systems degrading the structural integrity of nearby buildings, pipeline systems, sensitive instruments; additionally, small-scale damage to structures in petrochemical industries or nuclear reactors can have devastating consequences. Traditional approaches for vibration mitigation, mostly in the form of base isolation (BI) and tuned mass damper (TMDs) have certain limitations [5, 6, 7, 8, 9, 10]: BI induces large movement of the structures which may not be acceptable, TMD works only for a narrow frequency range outside of which it may work adversely which is again a major issue because identifying the frequency contents in the structure correctly is not straightforward as it may change significantly with time due to structural degradation and environmental change [11, 12].

In the parallel research area of electromagnetism, there is a keen interest in composites, known as metamaterials, which are assemblies of multiple elements usually arranged in periodic patterns at subwavelength scales, that were introduced [13] as a means to achieve effective electromagnetic prop-

erties not from the properties of the constituent materials, but from the combination of elements with given shapes and orientations, such as split ring resonators. Such periodically arranged elements take their name from the shape of the thin metal sheets they are made of that allow for artificial magnetism, not present in the constituent materials (metal surrounded by plastic, neither of which are magnetic media), through the precise manipulation of electric and magnetic components of electromagnetic field and their interplay. Indeed, the electromagnetic field is tremendously enhanced due to internal capacitance and inductance phenomena upon resonance of the thin sheets. From the highly dispersive nature of the metamaterials around the resonant frequencies of split ring resonators and other arrangements such as swiss-rolls, it is possible to block, absorb, enhance or even bend electromagnetic waves propagating through a doubly or triply periodic array of them, as low frequency stop bands and strong anisotropy (apparent in distorted isofrequency contours in pass bands) take place [14].

Metamaterials have the capability of manipulating a desired range of frequency components in the propagating wave, an aspect that has been extensively used in electromagnetics, optics and micro and nano-scale mechanics [15, 16, 17, 18, 19, 20, 21, 22, 23, 24, 25, 26]. However, their large scale extension, which can be extremely useful in solving many of the important engineering problems, mentioned above, requires development. Recent developments have indicated that metamaterials, if designed appropriately, can indeed provide a robust solution for elastic waves, thanks to their ability to create large frequency bandgaps even at large scale [27, 28, 29, 30, 31, 32, 33, 34, 35, 36, 37, 38, 39].

Early work by Economou and Sigalas [40] established a generic trend that a denser inclusion in the microstructure geometry of periodic media exhibits bandgaps for 2D and 3D structures. This phenomenon is predicted in [41, 42, 43] by using the Floquet-Bloch theory which is applicable to different wave types traveling through a periodic media. Experimentally [44, 45] showed the attenuation of surface elastic waves in a marble quarry containing repeated circular holes with the bandgaps obtained in a high frequency range of several kHz which is not important for seismic applications, because seismic forces mostly contain very low frequencies in the range of few Hz [46, 47, 48, 49]. The first full-scale experiments [29, 50] to attenuate surface elastic waves, such as Rayleigh and Love waves, were conducted in structured soil and extended in [30, 51, 52, 53]; the soil was engineered with cylindrically configured voids as inclusions in a periodic manner and this experiment shows

the feasibility of using phononic crystals and metamaterials at a meter-scale important for civil engineering applications.

A variety of extensions of these concepts are aimed at creating larger bandgaps and to force these to occur at the low frequencies required for civil engineering applications. Recently [54] numerically analyzed and designed optimal configuration for inclusions of micro-structure geometry, i.e., cross-shaped voids, hollow cylindrical and locally resonant inclusions (e.g. steel, rubber, concrete), which shield low frequency contents in seismic forces. Their parametric study on the filling fraction of inclusions in micro-structure shows a possibility of enhancing the bandgap. The ultimate goal of bandgap engineering in this context is to create a zero-frequency bandgap, i.e. one that starts at zero frequency and then extends over a broad range of low frequencies. [55] show that this can be achieved with cylindrical steel inclusions clamped to a bed rock which lies underneath a soil layer; they also considered struts linking the cylindrical steel columns.

Here we focus on large scale metamaterials made by periodically installing stiff columns in a matrix-like soil. There are many aspects that are not yet known about such metamaterials, e.g., effect of structure geometry, that is the detailed geometry within a single building block of the periodic medium, and material constituents. Although the possibility of enhancing the bandgap via varying the substitution ratio of stiffer inclusions is established, the effect of varying the structure geometry, keeping the same filling-fraction, is yet to be addressed. In the present study, we investigate the effect of the structure geometry in SMs with the aim of creating large bandgaps, keeping volume of inclusions same. As an illustrative example of the importance of structure geometry, we show in Figure 1 two similar geometries for SMs: we see in Figure A.18 that just simply tilting some junctions between a cylinder and a bulk medium has a profound impact on stop band width, as noted in earlier studies on phononic crystals consisting of inertial resonators [56, 57, 58]. We also explore the performance of SMs by considering different constituent materials. Specifically, we aim to maximize the bandgap width as well as the number of stopbands since the SMs may have to safeguard different types of civil installations with varied frequency contents ranging from massive tall buildings with very small natural frequencies to fluid conveyors containing large natural frequencies [59, 60]. En-route to enhancing the bandgap, we report an innovative design for SM, which is very pertinent to civil engineering practices. The rest of the paper is organized as follows: The mathematical formulation is shown in section 2 and consequently numerically simulated

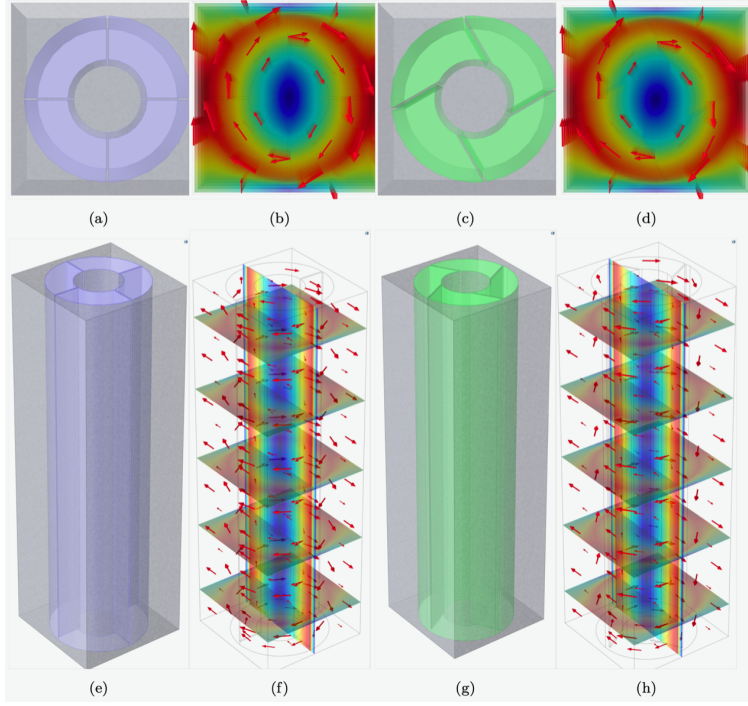


Figure 1: Unclamped cylindrical steel inclusion (radius  $r = 0.62$  m, height  $h = 10$  m) placed inside a cylindrical air cavity ( $r = 1.3$  m,  $h = 10$  m), surrounded by soil, inside an elementary cell ( $3\text{ m} \times 3\text{ m} \times 10\text{ m}$ ) with periodic boundary conditions on opposite vertical sides, thus structuring soil in a doubly periodic manner. Each steel cylinder is connected to the soil matrix with 4 ligaments (0.04 m thick steel plates, 10 m in height). When ligaments are aligned with the center of the cell (a,e), a rotational eigenmode (b,d) occurs at frequency 42 Hz. When ligaments are tilted by an angle of 30 degrees with respect to the center of the cell (c,g), the rotational eigenmode (d,h) is shifted to frequency 38.6 Hz.

results are given in section 3. Finally, we draw some conclusions in Section 4.

## 2 Mathematical Formulation-Finite Element Approach

We take an elastic medium consisting of isotropic homogeneous phases, for which the governing equation [61] is

$$(\lambda + \mu) \frac{\partial^2 u_j}{\partial x_j \partial x_i} + \mu \frac{\partial^2 u_i}{\partial x_j \partial x_j} = \rho \frac{\partial^2 u_i}{\partial t^2} \quad (1)$$

which is valid in each homogeneous phase, we use tensor notation. Eq. (1) is supplied with a no slip condition at the interface between the homogeneous phases, i.e., relative displacement will be zero between the phases as well as continuity of the normal component of stress to the interface. We work primarily in the frequency,  $\omega$ , domain and assume  $\exp(-i\omega t)$  dependence is considered understood and suppressed henceforth.

A periodic medium can be analyzed by sequential translational operations performed on its elementary cell, by making use of a lattice vector  $\mathbf{a} = (a_1, a_2)$ . The inherent periodicity of this cell enables us to characterize the dispersion properties of elastic waves propagating within such a periodic medium, via Bloch's theorem as in Eq.(2), where  $\mathbf{k} = \{k_x, k_y\}$  is the Bloch wavevector and  $\mathbf{x} = (x_1, x_2)$  [62]:

$$\mathbf{u}(\mathbf{x} + \mathbf{a}) = \mathbf{u}(\mathbf{x}) \exp(i\mathbf{k} \cdot \mathbf{a}) \quad (2)$$

and, to obtain, dispersion relations between frequency and phase-shift we need only consider the elementary cell.

For our numerical simulations we arrive at Eq. (3) by discretizing  $u$  in weak form using 3D shape functions in a finite element approach [63]:  $\mathbf{K}$  and  $\mathbf{M}$  being global stiffness and mass matrices, respectively, which are basically functions of Bloch wavevector  $\mathbf{k}$ , and  $\mathbf{U}$  is the assembled displacement vector.

$$(\mathbf{K} - \omega^2 \mathbf{M}) \mathbf{U} = 0 \quad (3)$$

Floquet-Bloch analysis is conducted by computing dispersion curves via varying  $\mathbf{k} = \{k_x, k_y\}$  along the edges of irreducible Brillouin zone (IBZ). For a square lattice, IBZ lies along the edges of the triangle  $\Gamma M X$ ;  $\Gamma = (0, 0)$ ,  $M = (\frac{\pi}{a}, \frac{\pi}{a})$  and  $X = (\frac{\pi}{a}, 0)$ , where  $a = a_1 = a_2$ . For a real valued  $\mathbf{k}$ , the frequencies ( $\omega$ ) are obtained by solving an appropriate eigenvalue problem, thereby constructing the dispersion curves via plotting real valued frequencies

corresponding to  $\mathbf{k}$  [64, 65]. Since dispersion curves are computed over a medium representing an infinite array of micro-structured geometry, they alone do not fully reveal the inherent effectiveness of SM design. For this purpose, transmission spectra are also computed, which is a measure of wave propagation attenuation/transmission losses over a finite medium [66].

### 3 Results and Discussion

In this section, we present dispersion curves and transmission losses for different microstructure geometries. To arrive at a microstructure that maximizes the bandgap, we compare different results keeping the substitution ratio the same. Having arrived at a particular configuration, we explore the effect of changes in orientation of the inclusion from  $0^\circ$  to  $45^\circ$ . After this we move to the aspect of material constituent for the inclusion and we also focus on cost effectiveness and ease of fabrication of arbitrary microstructure geometry.

#### 3.1 Comparison of different geometry of inclusions

Most standard civil engineering infrastructures are constructed on medium to dense soil, for their obvious stability purposes, and to reflect this we choose realistic soil conditions, i.e., medium soil with parameters as elastic modulus,  $E = 153$  MPa, Poisson's ratio,  $\mu = 0.3$  and density,  $\rho = 1800$  kg/m<sup>3</sup>. The micro-structure of the periodic media is configured with steel columns as inclusions in three forms having same substitution ratio as shown in Fig. 2.

- Cylindrical steel column of height 10 m and circular cross-section of radius 1.128 m.
- Regular sized square steel column of same height, i.e., 10 m. The cross-section of regular sized square is taken as  $2 \text{ m} \times 2 \text{ m}$ .
- Notch-shaped square steel column again with same height, i.e, 10 m.  $0.4 \text{ m} \times 0.6 \text{ m}$  notch is provided in a square of  $2.25 \text{ m}$  size as shown in Fig. 2e.

Each form of inclusion is embedded in unstructured medium soil matrix ( $3 \text{ m} \times 3 \text{ m} \times 10 \text{ m}$ ) so as to make an elementary cell that forms the microstructure of the periodic media; top and bottom of the microstructure remains unclamped for the simulations shown in Fig.2. Elastic properties

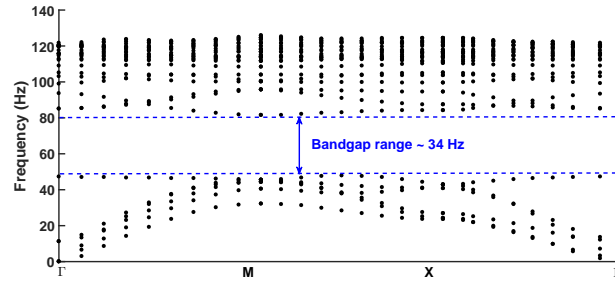
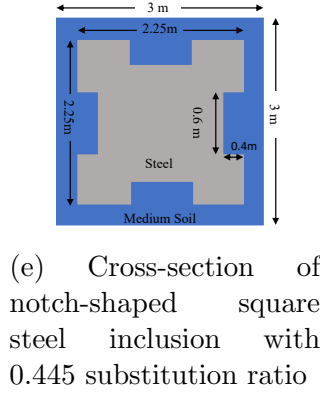
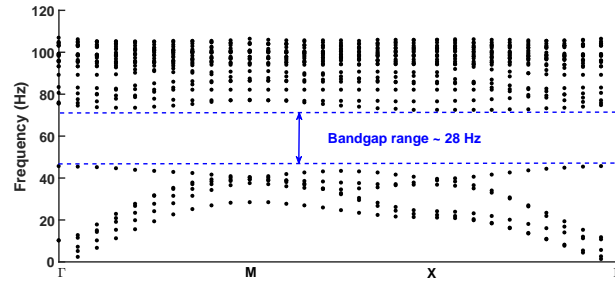
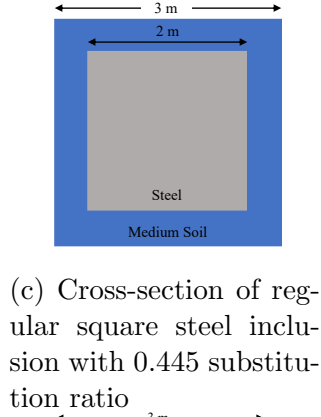
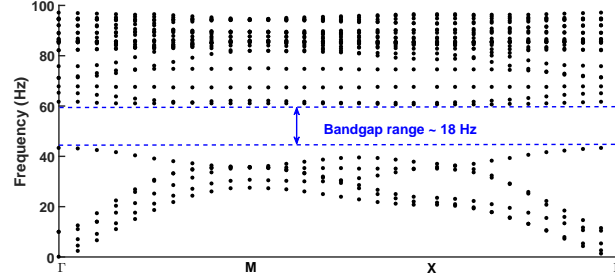
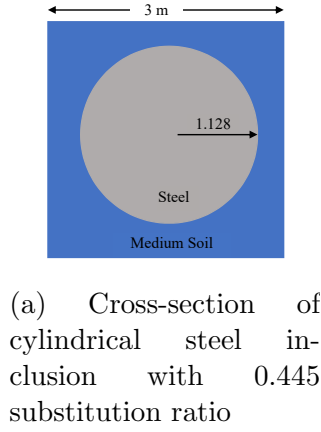


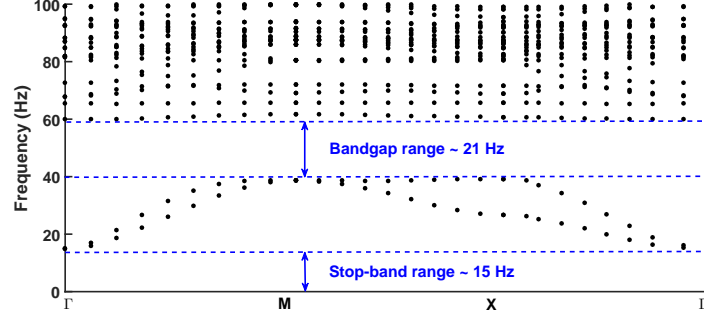
Figure 2: Unclamped configuration of (a) cylindrical ( $r = 1.128$  m,  $h = 10$  m), (c) regular-shaped square (2m x2m x10m) and (e) notch-shaped square geometry inclusions in the elementary cell (3m x3m x10m) of periodic media (medium soil) with equal substitution ratio (0.445). Dispersion curves for (b) cylindrical (d) regular-shaped square and (f) notch-shaped square inclusions are obtained around the edges of the irreducible Brillouin zone  $\Gamma XM$ . Note that there is an enhanced bandgap range with regular-shaped square (approx. 28 Hz) and notch-shaped square (approx. 34 Hz) inclusions in comparison to cylindrical inclusion (approx. 18 Hz).



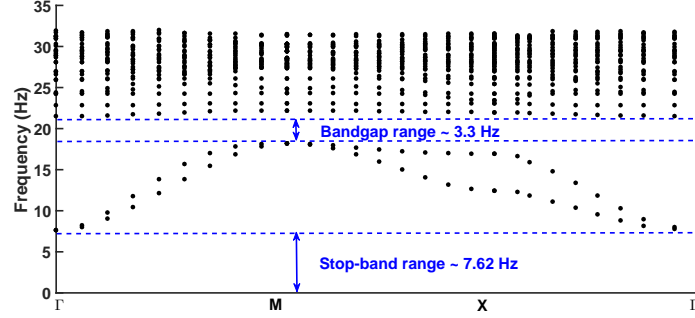
of steel are chosen as  $E = 200$  GPa, Poisson's ratio,  $\mu = 0.33$  and density,  $\rho = 7850$  kg/m<sup>3</sup>. We have also used soft clay models (which will be seen subsequently) to study the effect of soil on bandgap enhancement. A comparison of its dispersion properties, obtained along the edges of the irreducible Brillouin zone  $\Gamma MX$  (see section 2), can be made from Fig.2. Bandgaps are obtained in all the configurations, i.e., microstructure with inclusions having circular, regular square and notch-shaped square cross-sections. The square cross-section inclusions show a higher range of bandgap (approximately 28 Hz and 34 Hz in regular and notch-shaped, respectively) in comparison to circular cross-section inclusion (approximately 18 Hz) for the same substitution ratio of steel.

Comparison of stop-bands for these configurations are also obtained (see Fig.3), by clamping the bottom of the microstructure. Here, the column inclusions with circular cross-sections show better zero-frequency stop-bands (with upper limit at approximately 15 Hz) in contrast to regular square shaped inclusions (upper limit at approximately 7.62 Hz). However, the notch-shaped square inclusion shows a slightly higher stop-band (upper limit approximately 17 Hz) to that of circular cross-section for same substitution ratio of steel inclusion. Along with the zero-frequency stop-band, there is an additional bandgap at a higher frequency range that is also observed for all three forms of inclusions. The circular cross-section shows a higher frequency bandgap with a range of around 21 Hz in comparison to regular square shaped cross section which has only a narrow bandgap with a range of about 3.3 Hz. The notch-shaped square cross-section shows a slightly higher range of bandgaps, approximately 21.75 Hz (7.85 Hz + 14 Hz), than the circular cross-sectioned inclusion. However, the bandgaps for circular and notch-shaped inclusions are positioned in the higher frequency spectrum, which are less important for engineering applications.

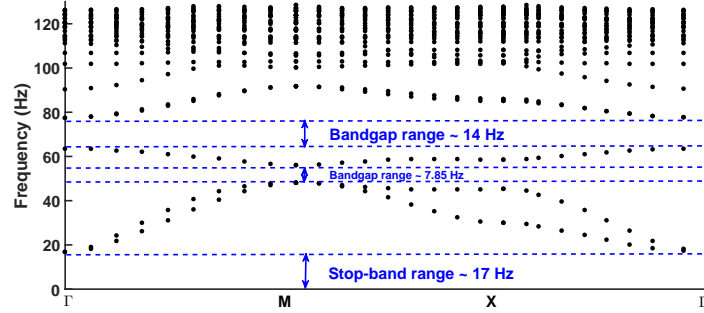
Motivated by the electromagnetic metamaterials literature, other investigated microstructure geometries are now considered: coil/Labyrinthine (complex sheet piling type of inclusion), split ring-like and swiss roll-like cylindrical steel inclusions in medium soil (see Fig. 4 and 5). The same substitution ratio, i.e., 0.445 was considered as in the former two microstructures, whereas the swiss roll-like inclusion is considered with a diameter equal to that of the solid circular inclusion in Fig.2, i.e., 1.128 m with a substitution ratio of 0.15. Notably, in medium soil, without clamping the bottom, a split-ring like inclusion with 4 gaps shows a bandgap of approximately 10.6 Hz, whereas the Labyrinthine inclusion shows no bandgap. Testing with other material con-



(a) Dispersion curves for circular cross-section with 1.128 m radius as shown in Fig. 2a



(b) Dispersion curves for regular-shaped square cross-section of side length 2 m as shown in Fig. 2c



(c) Dispersion curves for notch-shaped square cross-section (four notches of dimension 0.6 m  $\times$  0.4 m in a 2 m square as shown in Fig. 2e)

Figure 3: Dispersion curves for clamped configuration of geometries, i.e. the base of the inclusion column is clamped, shown in Fig.2 with the same substitution ratio 0.445. Notch-shaped square cross-section shows a higher stop-band than the other two geometries, however, the frequencies are lifted up in their comparison.

stituents for a Labyrinthine inclusion (Fig. 4a), i.e., with rubber and concrete no bandgap was observed (see Fig. 6). On the other hand, split-ring with 2 gaps shows an enhanced bandgap (12 Hz in the range of 46.84 Hz- 59.23 Hz) as compared to 4 gap split-ring (10.6 Hz in the range of 48.53 Hz- 58.35 Hz) with same substitution ratio (0.445). Dispersion curves for swiss roll-like steel inclusion with different thickness, i.e., 0.128 m and 0.03 m in medium soil ( $3\text{ m} \times 3\text{ m} \times 10\text{ m}$ ) is obtained by without clamping the bottom and is shown in Fig.5. Clearly, there is no bandgap for these configurations.

The stop-bands for the configurations in Fig.4 and 5 are obtained by clamping the bottom and are shown in Fig.7. It is observed that the Labyrinthine inclusion gives higher stop-bands in contrast to other two, i.e., 14.7 Hz for the Labyrinthine steel inclusion in comparison with 12.7 Hz and 11 Hz for split-ring and swiss-roll like steel inclusions.

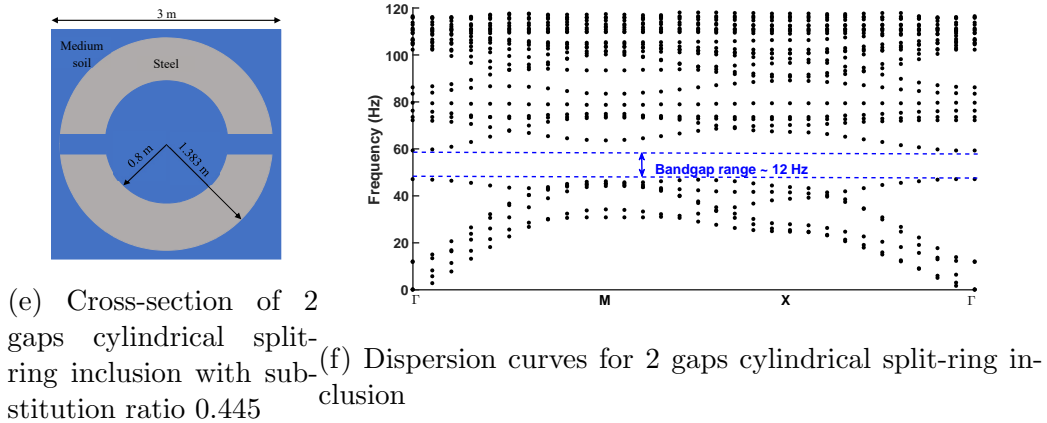
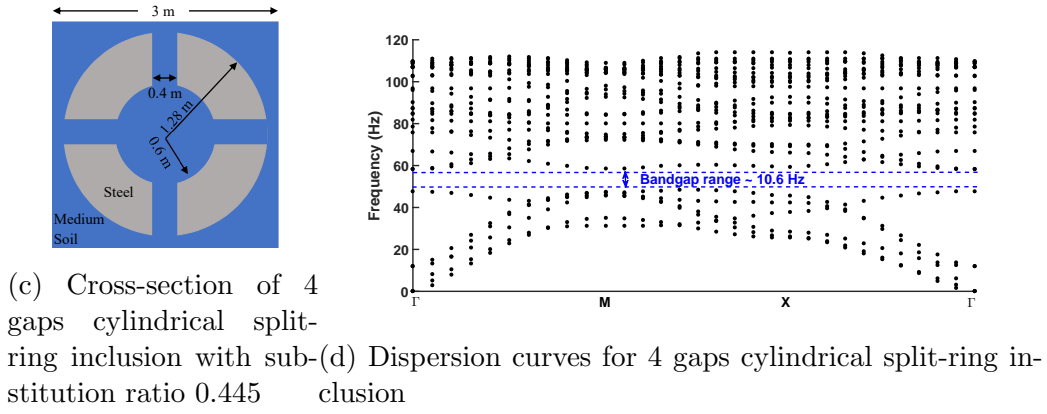
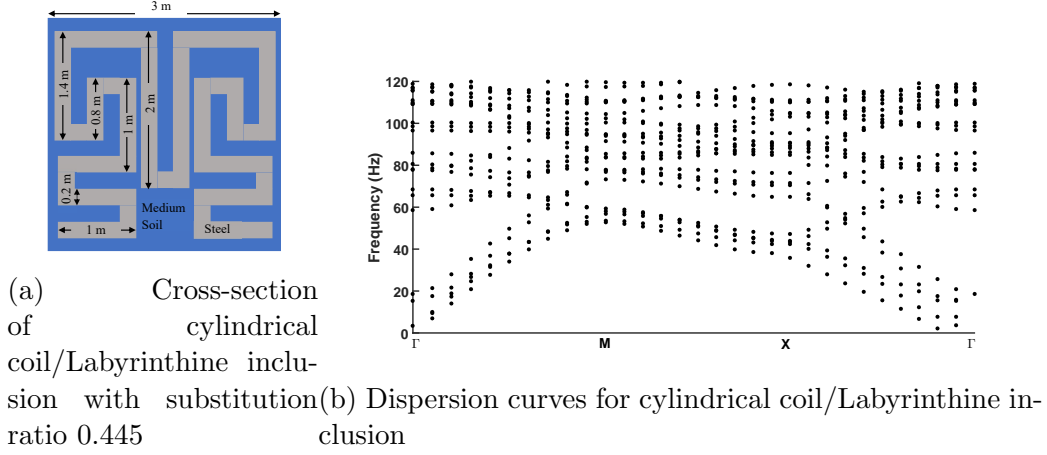
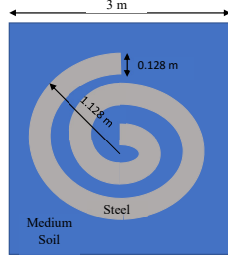
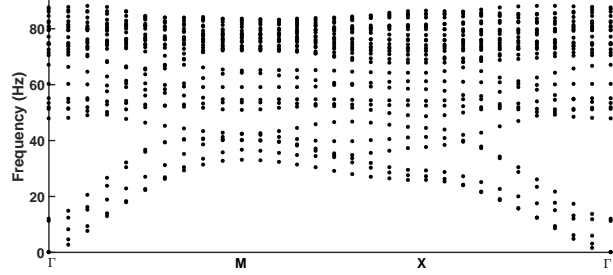


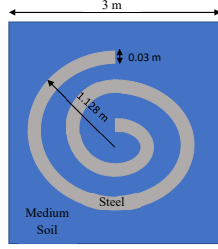
Figure 4: Unclamped configuration of (a) coil/Labyrinthine, (c) 4 gaps split-ring and (e) 2 gaps split-ring with steel as inclusion with substitution ratio 0.445 in the elementary cell (3m x3m x10m) of periodic media (medium soil). Corresponding dispersion curves obtained around the edges of the irreducible Brillouin zone  $\Gamma XM$  are shown aside (b, d, f). Labyrinthine inclusion shows no bandgap in medium soil, whereas split-ring with same substitution ratio shows bandgap in the range of 45 Hz - 60 Hz. Notably, split-ring with 2 gaps shows an enhanced bandgap (12 Hz in the range of 46.84 Hz- 59.23 Hz) as compared to 4 gap split-ring (10.6 Hz in the range of 48.53 Hz- 58.35 Hz).



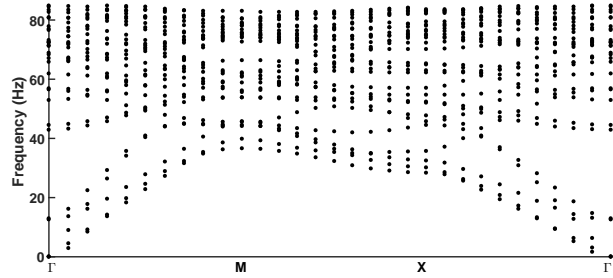
(a) Cross-section of cylindrical swiss roll-like inclusion with thickness 0.128 m



(b) Dispersion curves for cylindrical swiss roll inclusion with 0.128 m thickness

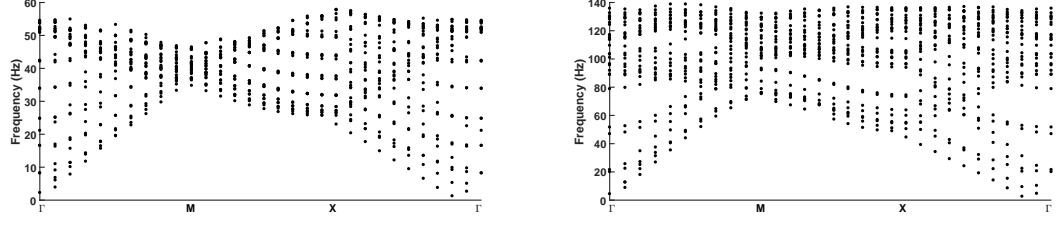


(c) Cross-section of cylindrical swiss roll inclusion with thickness 0.03 m



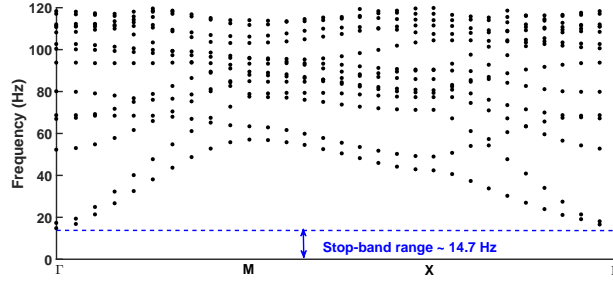
(d) Dispersion curves for cylindrical swiss roll-like inclusion with 0.03 m thickness

Figure 5: Unclamped configuration of cylindrical swiss roll like geometry with different thickness of steel inclusions in the elementary cell (3m x3m x10m) of periodic media (medium soil) . Diameter of swiss roll is considered same as solid circular inclusions in Fig.2. No bandgap is observed in both the cases

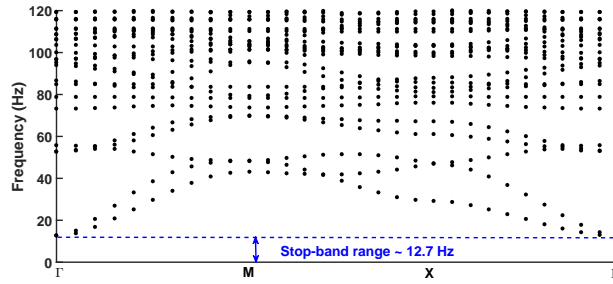


(a) Dispersion curve for Labyrinthine microstructure with rubber as inclusion (b) Dispersion curve for Labyrinthine microstructure with concrete as inclusion

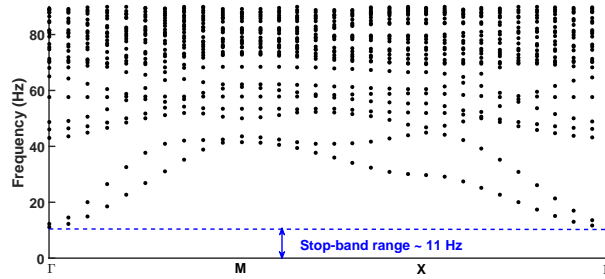
Figure 6: Dispersion curves for unclamped configuration of Labyrinthine geometry as shown in fig. 4a with different constituent material, i.e., (a) rubber and (b) concrete. No bandgap is observed with these inclusions



(a) Dispersion curves for cylindrical Labyrinthine inclusion

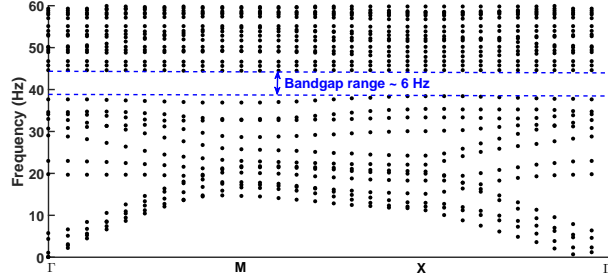


(b) Dispersion curves for cylindrical split-ring-like inclusion

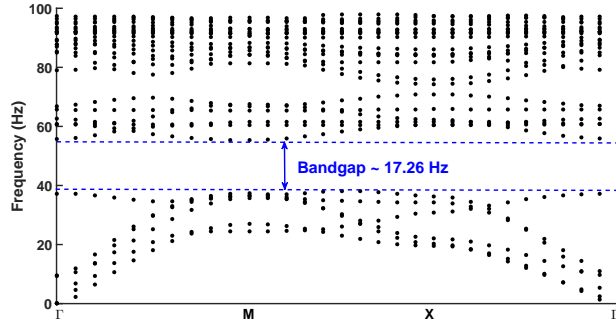


(c) Dispersion curves for cylindrical swiss-roll-like inclusion

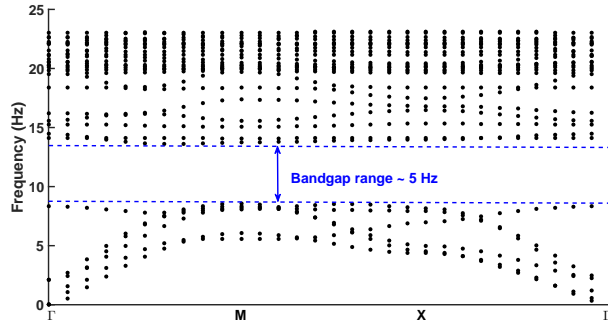
Figure 7: Dispersion curves for clamped configuration with steel as inclusion material for (a) Labyrinthine, (b) 4 gaps split ring, and (c) swiss roll with 0.128 m thickness with substitution ratio as 0.445 (for swiss roll: 0.15).



(a) Dispersion curves for cylindrical Labyrinthine inclusion in very soft clay type 1 (cross-section details in Fig. 4a)



(b) Dispersion curves for 2 gap cylindrical split-ring-like inclusion in soft soil (cross-section details in Fig. 4e)



(c) Dispersion curves for 2 gap cylindrical split-ring-like inclusion in very soft clay type 2 (cross-section details in Fig. 4e)

Figure 8: Dispersion curves for unclamped configurations of Labyrinthine and 2 gap split ring steel inclusions with 0.445 substitution ratio in soft ( $E = 96.5$  MPa,  $\mu = 0.33$  and  $\rho = 1650$  kg/m<sup>3</sup>), very soft clay type 1 ( $E = 10$  MPa,  $\mu = 0.25$  and  $\rho = 1400$  kg/m<sup>3</sup>) and very soft clay type 2 ( $E = 5$  MPa,  $\mu = 0.35$  and  $\rho = 1633$  kg/m<sup>3</sup>).



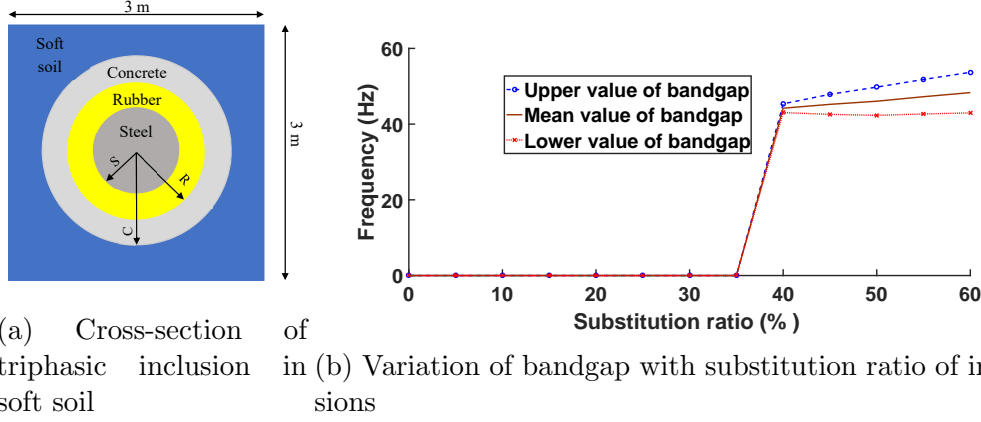


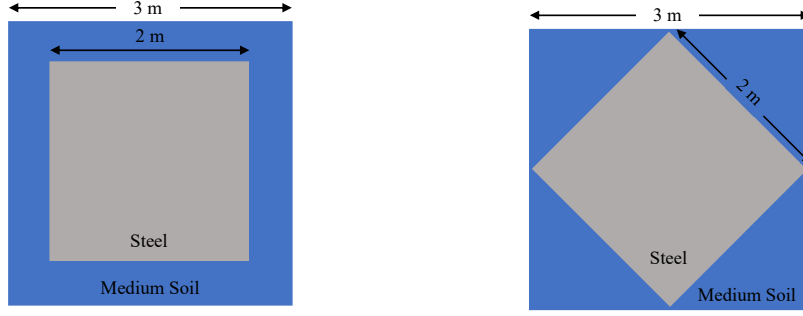
Figure 9: Unclamped configuration (all three type of inclusion, i.e., concrete, rubber and steel), and Variation of bandgap width versus substitution ratio of triphasic inclusion in soft soil. The ratio of radius of each inclusion material for different substitution ratio is kept same, i.e.,  $\frac{S}{R} = \frac{R}{C} = 0.83$ , where  $S$ ,  $R$  and  $C$  denotes radius of steel, rubber and concrete, respectively. The dimension of unit cell is  $3 \text{ m} \times 3 \text{ m} \times 10 \text{ m}$  and properties of soft soil is taken as  $E = 96.5 \text{ MPa}$ ,  $\mu = 0.33$  and  $\rho = 1650 \text{ kg/m}^3$ .

We now investigating the effect of different soil properties, i.e., with soft soil having properties  $E = 96.5 \text{ MPa}$ ,  $\mu = 0.33$  and  $\rho = 1650 \text{ kg/m}^3$  and very soft soil type 1 with properties  $E = 10 \text{ MPa}$ ,  $\mu = 0.25$  and  $\rho = 1400 \text{ kg/m}^3$ . The Labyrinthine and 2 gap split ring-like steel inclusions show an improvement on the width of the bandgaps obtained via dispersion curves in Fig. 4. The Labyrinthine steel inclusion shows a bandgap of 6 Hz in the range of 38 Hz - 44 Hz in soft soil (Fig. 8a) in contrast to medium soil (Fig. 4b), which shows no bandgap. Split ring with 2 gaps shows an enhanced bandgap (approx. 17 Hz) in soft soil with soil properties  $E = 96.5 \text{ MPa}$ ,  $\mu = 0.33$  and  $\rho = 1650 \text{ kg/m}^3$  (Fig. 8b). The bandgap is also obtained in a lower region than that obtained in the medium soil (Fig. 4f). On further exploring the soil properties, the 2 gap split ring shows an excellent improvement over the bandgap in a very soft soil type 2 with soil properties  $E = 5 \text{ MPa}$ ,  $\mu = 0.35$  and  $\rho = 1633 \text{ kg/m}^3$ . A bandgap of 5 Hz is obtained at a much lower region (approx. 8 Hz - 13 Hz) in very soft soil type 2 for 2 gap split ring (Fig. 8c). Finally, we investigate a typical configuration such as a triphasic inclusion as shown in Fig. 9 [67]. A circular cylinder of steel, surrounded by a thick rubber shell, surrounded by a concrete outer shell within a bulk of soft soil

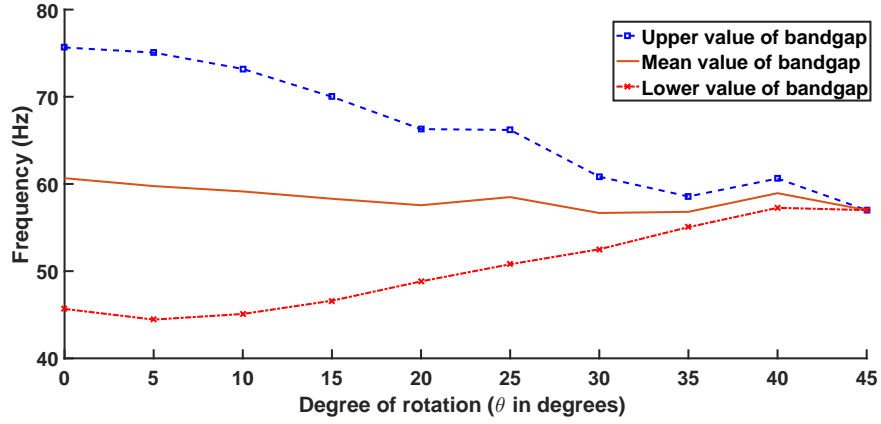
with parameters  $E = 96.5$  MPa,  $\mu = 0.33$  and  $\rho = 1650$  kg/m<sup>3</sup> as shown in Fig. 9a. The ratio of radius of each inclusion material is taken such as  $S/R = R/C = 0.83$ , where  $S, R$  and  $C$  denote radius of steel, rubber and concrete, respectively. The dimension of the unit cell is  $3 \text{ m} \times 3 \text{ m} \times 10 \text{ m}$ . With increasing substitution ratio of material constituents, the varying bandgap width is plotted as shown in Fig. 9b. It can be seen that the band gap for triphasic inclusion appears at lower substitution rates than for monophasic substitution cases.

### 3.2 Effect of varying orientation in square inclusions

Having verified in subsection 3.1, that using a square geometry as the inclusion leads to better performance, here we explore the effect of varying its orientation within the microstructure of periodic media by rotating it from  $0^\circ$  to  $45^\circ$ . With this exercise, we further explore the microstructure geometries towards achieving higher bandgaps. Steel inclusions are considered as the column with regular-shaped square geometry ( $2 \text{ m} \times 2 \text{ m} \times 10 \text{ m}$ ) within an unstructured medium soil ( $3 \text{ m} \times 3 \text{ m} \times 10 \text{ m}$ ), with properties same as in section 3.1. The orientation of the square inclusion is made to vary from  $0^\circ$  to  $45^\circ$ , in increments of  $5^\circ$ . Fig. 10c shows the plot for bandgaps obtained from varying the orientation of inclusion plotted against the angle. Interestingly, the plot shows a declining trend for the bandgap with increase in angle, starting from 28 Hz at  $0^\circ$  to 0 Hz at  $45^\circ$ . Thus, in summary a square inclusion oriented at  $0^\circ$  gives a wider bandgap in comparison to other orientations when examined with same substitution ratio. To further investigate the efficacy of the design, transmission losses (see Fig. 11) are computed over a finite array of SM design consisting of five square steel columns (oriented at  $0^\circ$  and  $45^\circ$ , respectively). For the computation, Rayleigh wave is incident normally as a line source. With  $0^\circ$  orientation a dip is observed in the range of 58 Hz-82 Hz, which shows possible large wave attenuation/transmission loss, whereas no such observations is made for the  $45^\circ$  case.



(a) Cross-section of  $0^\circ$  orientation of square inclusion with 0.445 substitution ratio (b) Cross-section of  $45^\circ$  orientation of square inclusion with 0.445 substitution ratio



(c) Bandgap for unclamped configuration versus orientation angle (degree) plot for square inclusion (steel) in medium soil at same substitution ratio, i.e., 0.445

Figure 10: Effect of change in orientation angle (in degrees) of unclamped regular-shaped square steel inclusion ( $2 \text{ m} \times 2 \text{ m} \times 10 \text{ m}$ ) with 0.445 substitution ratio in medium soil ( $3 \text{ m} \times 3 \text{ m} \times 10 \text{ m}$ ;  $E = 153 \text{ MPa}$ ,  $\mu = 0.33$  and  $\rho = 1800 \text{ kg/m}^3$ ) on bandgap; (a) and (b) shows the cross-section of  $0^\circ$  and  $45^\circ$  angle orientation of unclamped square inclusion; (c) shows the declining trend in bandgap with increase in angle from  $0^\circ$  to  $45^\circ$  in anticlockwise direction

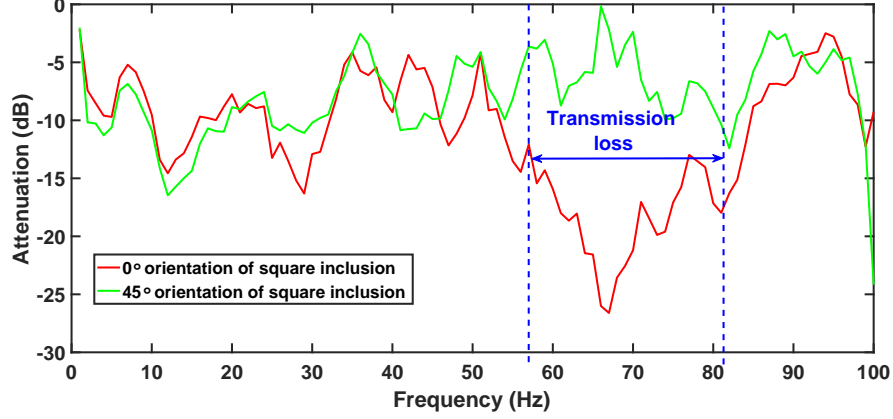
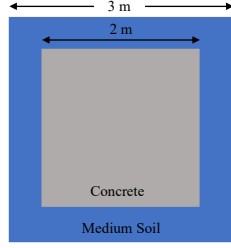


Figure 11: Transmission spectra of  $0^\circ$  and  $45^\circ$  orientation of square steel inclusion in medium soil matrix (bottom remains unclamped) is computed using a finite array of metamaterial design (Corresponding to Fig. 10). A dip is observed at approximately 68 Hz, representing large wave attenuation.

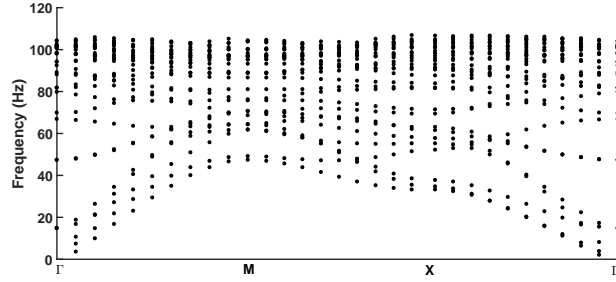
### 3.3 Feasibility of inclusion material

So far we have discussed the geometry of the inclusions within the unit cell, so as to generate a wide bandgap and its positioning in the frequency spectrum. However, we have exclusively utilized steel as the constituent material of the inclusion. But it is not feasible, either economically and technically, to generate such a large volume of steel having dimensions  $2 \text{ m} \times 2 \text{ m} \times 10 \text{ m}$  making up a volume of  $40 \text{ m}^3$  and then give them complex cross-section geometry via standard industrial fabrication processes. Conversely, concrete has an advantage over steel, in terms of fire and corrosion resistance, low density, resistant to impact of high groundwater level and other on-field applications like being easily mouldable into desired shapes, and these considerations make it a better choice within the civil engineering domain. Noting this fact, we compared the dispersion properties of concrete inclusions (M50 grade) with that of steel inclusions (Figs. 2d and 12b); both having same substitution ratio (0.445) and embedded in medium soil whose geometry and elastic properties are same as in section 3.1. The elastic properties of M50 grade concrete is taken as  $E = 35.35 \text{ GPa}$ , Poisson's ratio,  $\mu = 0.15$  and density,  $\rho = 2400 \text{ kg/m}^3$ . Unfortunately, concrete inclusions in medium

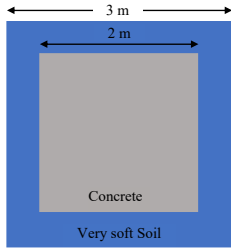
soil matrix show no bandgap frequencies (Fig. 12b). However, as discussed earlier, concrete is an ideal choice for most of the civil installations, and so we performed a parametric study with different grades of concrete combined with soft, medium and dense soil. In the process of which, we arrive at a design of SM having M50 grade concrete inclusion in very soft soil type 1 (soil properties is taken as  $E = 10$  MPa, Poisson's ratio,  $\mu = 0.25$  and density,  $\rho = 1400$  kg/m<sup>3</sup>), showing a bandgap of approximately 3.91 Hz in the range of 18.45 Hz-22.36 Hz (Fig. 12d). Transmission loss are computed using a finite strip of five concrete square columns in very soft soil type 1 which shows large Rayleigh wave attenuation in range of 15 Hz- 25 Hz, in comparison to medium soil (Fig. 13). Zero frequency stop-band computation (see Fig. 14) distinctly shows two bandgaps; ultra-low stop-band frequency (0-7.62 Hz) and a higher range of bandgap, approximately 3.28 Hz (range 18.72 Hz-22 Hz). Transmission loss for 0° oriented regular-shaped square concrete columns in very soft soil type 1 ( $E = 10$  MPa,  $\mu = 0.25$  and  $\rho = 1400$  kg/m<sup>3</sup>) and medium ( $E = 153$  MPa,  $\mu = 0.3$  and  $\rho = 1800$  kg/m<sup>3</sup>) soil matrix is also computed over a finite array of the design region (see Fig. 15). Clearly, concrete columns in soft soil type 1 attenuates the Rayleigh wave vibrations to a larger extent in comparison to medium soil matrix in stop-band.



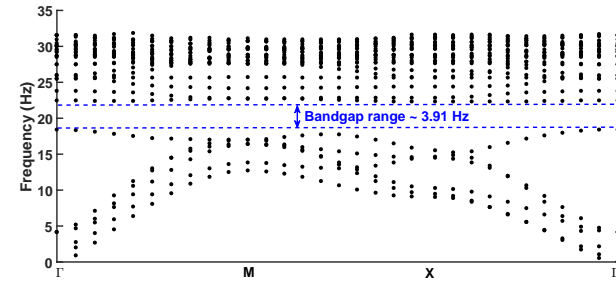
(a) Concrete inclusion in medium soil matrix with 0.445 substitution ratio



(b) Dispersion curves for square inclusion in medium soil



(c) Concrete inclusion in very soft soil matrix with 0.445 substitution ratio



(d) Dispersion curves for square inclusion in loose soil

Figure 12: Unclamped configuration of concrete inclusion (with 0.445 substitution ratio) in (a) medium soil ( $E = 153$  MPa,  $\mu = 0.33$  and  $\rho = 1800$  kg/m<sup>3</sup>); (c) very soft soil ( $E = 10$  MPa,  $\mu = 0.25$  and  $\rho = 1400$  kg/m<sup>3</sup>). Corresponding dispersion curves obtained are shown in (b) and (d), around the edges of the irreducible Brillouin zone  $\Gamma XM$ . No bandgap is observed with medium soil matrix; whereas in very soft soil a bandgap, approximately 3.91 Hz is observed.

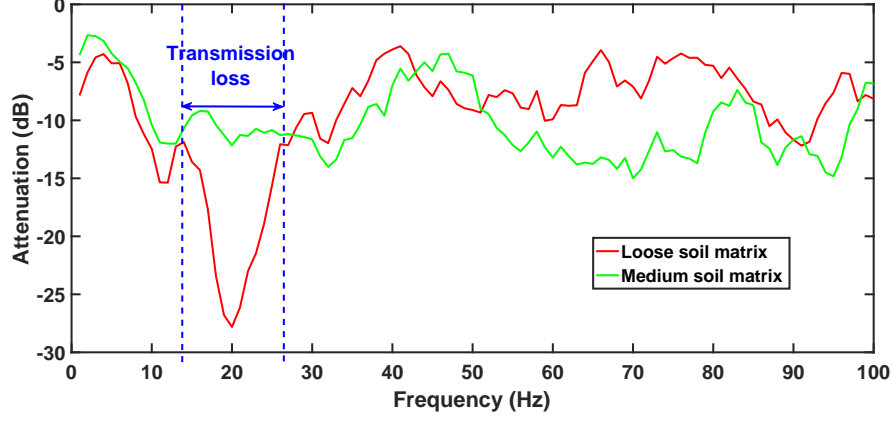


Figure 13: Transmission losses for unclamped concrete inclusions ( $2 \text{ m} \times 2 \text{ m} \times 10 \text{ m}$ ) in very soft soil type 1 ( $E = 10 \text{ MPa}$ ,  $\mu = 0.25$  and  $\rho = 1400 \text{ kg/m}^3$ ) and medium soil ( $E = 153 \text{ MPa}$ ,  $\mu = 0.33$  and  $\rho = 1800 \text{ kg/m}^3$ ) matrix ( $3 \text{ m} \times 3 \text{ m} \times 10 \text{ m}$ ) corresponding to Fig. 12. The substitution ratio is kept same, i.e., 0.445. Notably, square concrete inclusions in very soft soil type 1 shows attenuation in the bandgap range, i.e., 18.45 Hz-22.36 Hz.

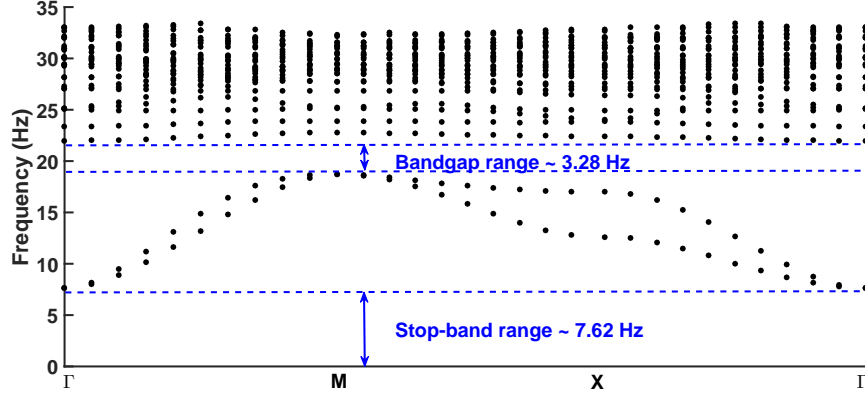


Figure 14: Dispersion curve for clamped configuration of M50 grade square concrete columns ( $2 \text{ m} \times 2 \text{ m} \times 10 \text{ m}$ ) in soft soil matrix ( $3 \text{ m} \times 3 \text{ m} \times 10 \text{ m}$ ;  $E = 10 \text{ MPa}$ ,  $\mu = 0.25$  and  $\rho = 1400 \text{ kg/m}^3$ ) (substitution ratio 0.445). Two bandgaps were observed; a stopband of 7.62 Hz and a bandgap in the range of 18.72-22 Hz



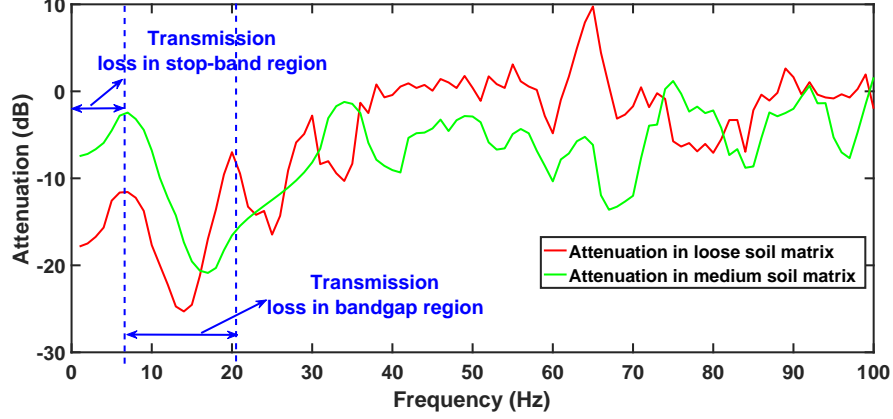


Figure 15: Attenuation for clamped configuration of square concrete columns having dimension  $2 \text{ m} \times 2 \text{ m} \times 10 \text{ m}$  in soft soil type 1 ( $E = 10 \text{ MPa}$ ,  $\mu = 0.25$  and  $\rho = 1400 \text{ kg/m}^3$ ) and medium soil ( $E = 153 \text{ MPa}$ ,  $\mu = 0.33$  and  $\rho = 1800 \text{ kg/m}^3$ ) matrix having dimension  $3 \text{ m} \times 3 \text{ m} \times 10 \text{ m}$  (substitution ratio 0.445). Clearly, loss in soft soil type 1 matrix is more in comparison to medium soil.

As mentioned earlier, since loose soil is not suitable for construction purpose, we recommend the following architecture. As shown in Fig. 16, for a finite region to be protected (denoted with A in Fig. 16), the SM microstructure should be designed using square inclusions of concrete columns oriented at  $0^\circ$  in a narrow strip of very soft soil matrix denoted with orange color in Fig. 16, leaving the residual region in its natural/structured state, making civil constructions possible on the residual region. Another aspect is that since the civil installations within the protected region may vary largely, with varied natural frequency range and importance, concrete columns of such a high dimension may not be necessary always. For the same, a parametric study on obtaining stop-bands with different concrete sizes is performed and the results are shown in Fig. 17. The effect of variation of stop-band follows a linear trend with increasing substitution ratio of regular-shaped square concrete columns. Such graphs can be used for calibration purpose for optimal SM design.

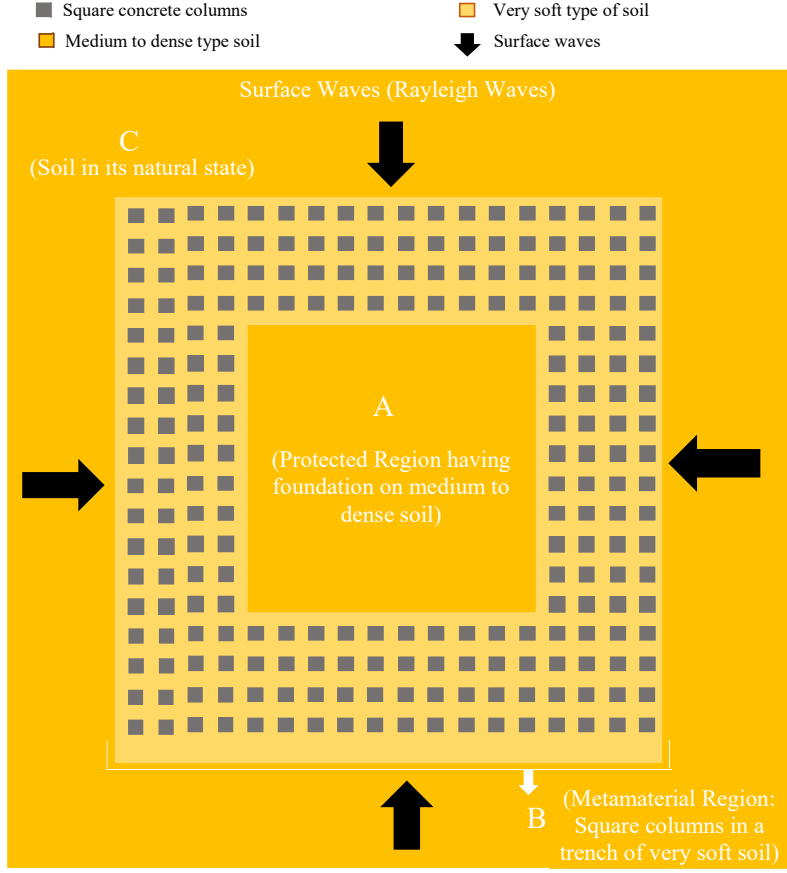


Figure 16: Schematic representation of the proposed design for metamaterial. Square columns of M50 grade embedded in loose soil matrix with properties,  $E = 10$  MPa,  $\mu = 0.25$  and  $\rho = 1400$  kg/m<sup>3</sup> are placed along a trench surrounding the protected area. The square concrete columns have substitution ratio 0.445 in the unit cell and are not clamped to the bottom.

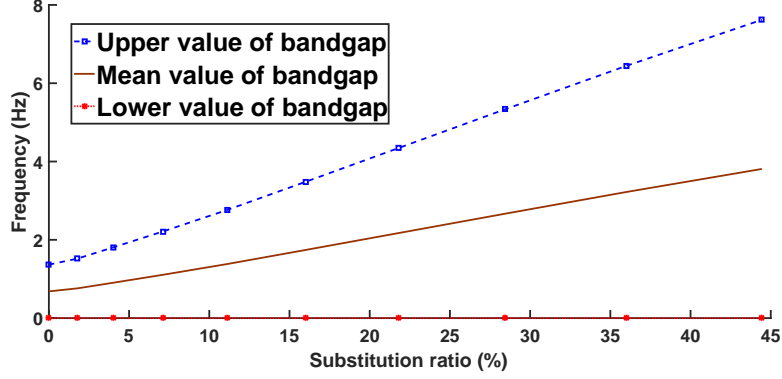


Figure 17: Bandgap versus substitution ratio plot for clamped configuration of square concrete inclusion in a unit cell of dimension  $3 \text{ m} \times 3 \text{ m}$ . The soil properties are taken as  $E = 10 \text{ MPa}$ ,  $\mu = 0.25$  and  $\rho = 1400 \text{ kg/m}^3$ .

## 4 Conclusion

In this paper, we have explored the effect of different microstructure geometries of SMs towards obtaining a wider bandgap with equal amount of inclusions and its positioning in frequency spectrum, i.e., a lower bandgap region (approx. below 20 Hz) is essential for most of the engineering applications. We have arrived at a configuration of columns having a square cross-section with sides aligned with the square lattice, that gives a wider bandgap in comparison to circular cross-section inclusions for same substitution ratio of constituent material. This has been demonstrated by computing transmission losses in addition to the dispersion curves for different microstructure geometries of the SM. We have also performed analysis of the constituent material, observing that, not only steel, but concrete the conventional construction material, can also be used to design inclusions for large wave attenuation. This is important for the industrial scale-up of the technology because, concrete is cost effective, easy to cast directly at the construction site and easy to provide arbitrary geometry of the microstructure. We have observed that concrete shows a bandgap for very soft soil. Since, very soft soil is not suitable for constructions, we prescribe an architecture of SM, with concrete inclusions in a narrow strip of very soft soil matrix surrounding the protected region. Even though we have arrived at an efficient design of SM,

our study open the door to further generalisation. For example, we assume linear elastic materials and it would be interesting to see what happens in case of material and geometric nonlinearity; soil often shows a significant amount of plastic deformation. In a future study, we would like to pay more attention to damping of ground vibrations, introducing so-called K-Dampers such as used to reduce vibration of bridges [68] and to mitigation of site-city interactions [30] using the SMs which we introduce here.

## Acknowledgement

Saikat Sarkar acknowledges Ravi Sharma and Anshul Srivastava (IIT Indore, B.Tech batch 2020) for helping him in some initial simulations at the preliminary stage of this work.

## References

- [1] T. Bajcar, F. Cimerman, B. Širok, M. Ameršek, Impact assessment of traffic-induced vibration on natural gas transmission pipeline, *Journal of Loss Prevention in the process industries* 25 (6) (2012) 1055–1068.
- [2] J. M. Brownjohn, A. De Stefano, Y.-L. Xu, H. Wenzel, A. E. Aktan, Vibration-based monitoring of civil infrastructure: challenges and successes, *Journal of Civil Structural Health Monitoring* 1 (3-4) (2011) 79–95.
- [3] J. Zhang, Z. Liang, D. Feng, C. Zhang, C. Xia, Y. Tu, Response of the buried steel pipeline caused by perilous rock impact: Parametric study, *Journal of Loss Prevention in the Process Industries* 43 (2016) 385–396.
- [4] J. Yao, R. Zhao, N. Zhang, D. Yang, Vibration isolation effect study of in-filled trench barriers to train-induced environmental vibrations, *Soil Dynamics and Earthquake Engineering* 125 (2019) 105741.

- [5] X. Zhou, W. Yan, R. Yang, Seismic base isolation, energy dissipation and vibration control of building structures, *Journal of Building Structures* 23 (2) (2002) 2–13.
- [6] H. Xiang, Z. Shi, S. Wang, Y. Mo, Periodic materials-based vibration attenuation in layered foundations: experimental validation, *Smart Materials and Structures* 21 (11) (2012) 112003.
- [7] P. Xiang, A. Nishitani, Seismic vibration control of building structures with multiple tuned mass damper floors integrated, *Earthquake Engineering & Structural Dynamics* 43 (6) (2014) 909–925.
- [8] P. S. Harvey Jr, K. C. Kelly, A review of rolling-type seismic isolation: Historical development and future directions, *Engineering Structures* 125 (2016) 521–531.
- [9] H. Anajafi, R. A. Medina, Comparison of the seismic performance of a partial mass isolation technique with conventional tmd and base-isolation systems under broad-band and narrow-band excitations, *Engineering Structures* 158 (2018) 110–123.
- [10] C. Fabrizio, A. M. de Leo, A. Di Egidio, Tuned mass damper and base isolation: a unitary approach for the seismic protection of conventional frame structures, *Journal of Engineering Mechanics* 145 (4) (2019) 04019011.

- [11] P.-R. Wagner, V. K. Dertimanis, E. N. Chatzi, J. L. Beck,  
Robust-to-uncertainties optimal design of seismic metamaterials, *Journal of Engineering Mechanics* 144 (3) (2017) 04017181.
- [12] P. Moser, B. Moaveni, Environmental effects on the identified natural frequencies of the dowling hall footbridge, *Mechanical Systems and Signal Processing* 25 (7) (2011) 2336–2357.
- [13] J. Pendry, A. Holden, D. Robbins, W. Stewart, Magnetism from conductors and enhanced nonlinear phenomena, *IEEE transactions on microwave theory and techniques* 47 (11) (1999) 2075–2084.
- [14] M. Kadic, T. Buckmann, R. Schittny, M. Wegener, Metamaterials beyond electromagnetism, *Reports on Progress in physics* 76 (12) (2013) 126501.
- [15] C. M. Watts, X. Liu, W. J. Padilla, Metamaterial electromagnetic wave absorbers, *Advanced materials* 24 (23) (2012) OP98–OP120.
- [16] O. Casablanca, G. Ventura, F. Garescì, B. Azzerboni, B. Chiaia, M. Chiappini, G. Finocchio, Seismic isolation of buildings using composite foundations based on metamaterials, *Journal of Applied Physics* 123 (17) (2018) 174903.
- [17] R. V. Craster, S. Guenneau, Acoustic metamaterials: Negative refraction, imaging, lensing and cloaking, Vol. 166, Springer Science & Business Media, 2012.

- [18] S. Guenneau, A. Movchan, G. Pétursson, S. A. Ramakrishna, Acoustic metamaterials for sound focusing and confinement, *New Journal of physics* 9 (11) (2007) 399.
- [19] A. Poddubny, I. Iorsh, P. Belov, Y. Kivshar, Hyperbolic metamaterials, *Nature photonics* 7 (12) (2013) 948.
- [20] M. Kadic, A. Diatta, T. Frenzel, S. Guenneau, M. Wegener, Metamaterials beyond electromagnetism, *Physical Review B* 99 (21) (2019) 214101.
- [21] S. Brûlé, S. Enoch, S. Guenneau, Role of nanophotonics in the birth of seismic megastructures, *Nanophotonics* 8 (10) (2019) 1591–1605.
- [22] Y. Zeng, Y. Xu, H. Yang, M. Muzamil, R. Xu, K. Deng, P. Peng, Q. Du, A matryoshka-like seismic metamaterial with wide band-gap characteristics, *International Journal of Solids and Structures* 185 (2020) 334–341.
- [23] S. Brûlé, S. Enoch, S. Guenneau, R. Craster, Seismic metamaterials: controlling surface Rayleigh waves using analogies with electromagnetic metamaterials, *Handbook of metamaterials*, World Scientific (2018).
- [24] S. Brûlé, B. Ungureanu, Y. Achaoui, A. Diatta, R. Aznavourian, T. Antonakakis, R. Craster, S. Enoch, S. Guenneau, Metamaterial-like transformed urbanism, *Innovative Infrastructure Solutions* 2 (1) (2017) 20.
- [25] A. Colombi, R. V. Craster, D. Colquitt, Y. Achaoui, S. Guenneau, P. Roux, M. Rupin, Elastic wave control beyond band-gaps: shaping the flow of waves in plates and half-spaces with subwavelength resonant rods, *Frontiers in*

Mechanical Engineering 3 (2017) 10.

- [26] Y. Yang, H. Wang, F. Yu, Z. Xu, H. Chen, A metasurface carpet cloak for electromagnetic, acoustic and water waves, *Scientific reports* 6 (2016) 20219.
- [27] A. Palermo, S. Krödel, A. Marzani, C. Daraio, Engineered metabarrier as shield from seismic surface waves, *Scientific reports* 6 (1) (2016) 1–10.
- [28] Y. Liu, J. Huang, Y. Li, Z. Shi, Trees as large-scale natural metamaterials for low-frequency vibration reduction, *Construction and Building Materials* 199 (2019) 737–745.
- [29] S. Brûlé, E. Javelaud, S. Enoch, S. Guenneau, Experiments on seismic metamaterials: molding surface waves, *Physical review letters* 112 (13) (2014) 133901.
- [30] B. Ungureanu, S. Guenneau, Y. Achaoui, A. Diatta, M. Farhat, H. Hutridurga, R. V. Craster, S. Enoch, S. Brûlé, The influence of building interactions on seismic and elastic body waves, *EPJ Applied Metamaterials* 6 (2019) 18.
- [31] A. Colombi, D. Colquitt, P. Roux, S. Guenneau, R. V. Craster, A seismic metamaterial: The resonant metawedge, *Scientific reports* 6 (2016) 27717.
- [32] P. Moitra, B. A. Slovick, W. Li, I. I. Kravchenko, D. P. Briggs, S. Krishnamurthy, J. Valentine, Large-scale all-dielectric metamaterial perfect reflectors, *ACS Photonics* 2 (6) (2015) 692–698.



- [33] N. Aravantinos-Zafiris, M. Sigalas, Large scale phononic metamaterials for seismic isolation, *Journal of Applied Physics* 118 (6) (2015) 064901.
- [34] M. Mosby, K. Matouš, Computational homogenization at extreme scales, *Extreme Mechanics Letters* 6 (2016) 68–74.
- [35] B. Ungureanu, Y. Achaoui, S. Enoch, S. Brûlé, S. Guenneau, Auxetic-like metamaterials as novel earthquake protections, *arXiv preprint arXiv:1510.08785* (2015).
- [36] A. Diatta, Y. Achaoui, S. Brûlé, S. Enoch, S. Guenneau, Control of Rayleigh-like waves in thick plate Willis metamaterials, *AIP Advances* 6 (12) (2016) 121707.
- [37] F. Sun, L. Xiao, Bandgap characteristics and seismic applications of inerter-in-lattice metamaterials, *Journal of Engineering Mechanics* 145 (9) (2019) 04019067.
- [38] Muhammad, C. Lim, Elastic waves propagation in thin plate metamaterials and evidence of low frequency pseudo and local resonance bandgaps, *Physics Letters A* 383 (23) (2019) 2789–2796.
- [39] D. Del Vescovo, I. Giorgio, Dynamic problems for metamaterials: review of existing models and ideas for further research, *International Journal of Engineering Science* 80 (2014) 153–172.
- [40] E. Economou, M. Sigalas, Classical wave propagation in periodic structures: Cermet versus network topology, *Physical Review B* 48 (18) (1993) 13434.

- [41] D. Mandelik, H. Eisenberg, Y. Silberberg, R. Morandotti, J. Aitchison,  
Band-gap  
structure of waveguide arrays and excitation of Floquet-Bloch solitons,  
Physical review letters 90 (5) (2003) 053902.
- [42] J. Gazalet, S. Dupont, J. Kastelik, Q. Rolland, B. Djafari-Rouhani, A  
tutorial  
survey on waves propagating in periodic media: Electronic, photonic  
and  
phononic crystals. perception of the Bloch theorem in both real and  
fourier  
domains, Wave Motion 50 (3) (2013) 619–654.
- [43] A. Gómez-León, G. Platero, Floquet-Bloch theory and topology in  
periodically driven lattices, Physical review letters 110 (20) (2013)  
200403.
- [44] F. Meseguer, M. Holgado, D. Caballero, N. Benaches, J. Sánchez-  
Dehesa,  
C. López, J. Llinares, Rayleigh-wave attenuation by a semi-infinite  
two-dimensional elastic-band-gap crystal, Physical Review B 59 (19)  
(1999)  
12169.
- [45] F. Meseguer, M. Holgado, D. Caballero, N. Benaches, C. Lopez,  
J. Sanchez-Dehesa, J. Llinares, Two-dimensional elastic bandgap crystal  
to  
attenuate surface waves, Journal of lightwave technology 17 (11) (1999)  
2196–2201.
- [46] M. R. Gadallah, R. L. Fisher, Applied seismology: A comprehensive  
guide to  
seismic theory and application, PennWell Books, 2005.

- [47] S. L. Kramer, Geotechnical Earthquake Engineering, Pearson Education, Inc., 2007.
- [48] S. Chestler, K. Creager, Evidence for a scale-limited low-frequency earthquake source process, *Journal of Geophysical Research: Solid Earth* 122 (4) (2017) 3099–3114.
- [49] M. Nakano, T. Hori, E. Araki, S. Kodaira, S. Ide, Shallow very-low-frequency earthquakes accompany slow slip events in the Nankai subduction zone, *Nature communications* 9 (1) (2018) 1–8.
- [50] S. Brûlé, E. H. Javelaud, S. Enoch, S. Guenneau, Flat lens effect on seismic waves propagation in the subsoil, *Scientific reports* 7 (1) (2017) 18066.
- [51] S. Brûlé, S. Enoch, S. Guenneau, Emergence of seismic metamaterials: current state and future perspectives, *Physics Letters A* 384 (1) (2020) 126034.
- [52] S. Brûlé, S. Guenneau, The role of seismic metamaterials on soil dynamics, *arXiv preprint arXiv:1912.12916* (2019).
- [53] S. Brûlé, S. Enoch, S. Guenneau, Experimental evidence of auxetic features in seismic metamaterials: Ellipticity of seismic rayleigh waves for subsurface architected ground with holes, *arXiv preprint arXiv:1809.05841* (2018).

- [54] M. Miniaci, A. Krushynska, F. Bosia, N. M. Pugno, Large scale mechanical metamaterials as seismic shields, *New Journal of Physics* 18 (8) (2016) 083041.
- [55] Y. Achaoui, T. Antonakakis, S. Brule, R. Craster, S. Enoch, S. Guenneau, Clamped seismic metamaterials: ultra-low frequency stop bands, *New Journal of Physics* 19 (6) (2017) 063022.
- [56] D. Bigoni, S. Guenneau, A. Movchan, M. Brun, Elastic metamaterials with inertial locally resonant structures: Application to lensing and localization, *Physical Review B* 87 (17) (2013) 174303.
- [57] P. Wang, F. Casadei, S. Shan, J. Weaver, K. Bertoldi, Harnessing buckling to design tunable locally resonant acoustic metamaterials, *Physical Review Letters* 113 (1) (2014) 014301.
- [58] P. Wang, L. Lu, K. Bertoldi, Topological phononic crystals with one-way elastic edge waves, *Physical Review Letters* 115 (10) (2015) 104302.
- [59] C. L. Dym, H. E. Williams, Estimating fundamental frequencies of tall buildings, *Journal of Structural Engineering* 133 (10) (2007) 1479–1483.
- [60] C. L. Dym, Approximating frequencies of tall buildings, *Journal of Structural Engineering* 139 (2) (2012) 288–293.
- [61] J. D. Achenbach, *Wave Propagation in Elastic Solids*, North-Holland, Amsterdam, 1973.

- [62] L. Brillouin, Wave propagation in periodic structures: electric filters and crystal lattices, Courier Corporation, 2003.
- [63] J. N. Reddy, An introduction to the finite element method, New York (1993).
- [64] N. Van Der Aa, H. Ter Morsche, R. Mattheij, Computation of eigenvalue and eigenvector derivatives for a general complex-valued eigensystem, Electronic Journal of Linear Algebra 16 (1) (2007) 26.
- [65] E. Jarlebring, G. Mele, O. Runborg, The waveguide eigenvalue problem and the tensor infinite Arnoldi method, SIAM Journal on Scientific Computing 39 (3) (2017) A1062–A1088.
- [66] H. M. Lee, J. C. Wu, Transmittance spectra in one-dimensional superconductor-dielectric photonic crystal, Journal of Applied Physics 107 (9) (2010) 09E149.
- [67] F. Duplan, A. Abou-Chakra, A. Turatsinze, G. Escadeillas, S. Brûlé, F. Masse, Prediction of modulus of elasticity based on micromechanics theory and application to low-strength mortars, Construction and Building Materials 50 (2014) 437–447.
- [68] E. Sapountzakis, P. Syrimi, I. Antoniadis, Engineered metabarrier as shield from seismic surface waves, International Journal of Geoengineering Case Histories 4 (4) (2018) 289–305.

## A Material Properties

For convenience we summarize the geometry and elastic properties of the microstructures in the following tables.

Table 1: Geometry of the microstructures

Types	Width/thickness (m)	Length (m)	Diameter (m)	Substitution ratio
Medium soil	3	3	-	-
Loose soil	3	3	-	-
Circular inclusion	-	-	1.128	0.445
Regular shaped square inclusion	2	2	-	0.445
Notch shaped square inclusion	2.25	2.25	-	0.445
Labyrinthine like inclusion	0.2	7	-	0.445
4 gap split ring inclusion	-	-	Outer 1.28 Inner 0.6	0.445
2 gap split ring inclusion	-	-	Outer 1.383 Inner 0.8	0.445
Swiss roll 1	0.128	-	1.128	0.445
Swiss roll 2	0.03	-	1.128	0.15
Seismic resonant inclusion	-	-	0 - 1.311	0 - 0.6

Table 2: Material properties

Material	Elastic modulus (MPa)	Poisson's ratio	Density (kg/m3)
Medium soil	153	0.3	1800
Soft soil	96.5	0.33	1650
Very soft clay type 1	10	0.25	1400
Very soft clay type 2	5	0.35	1633
Steel	200.000	0.33	7850
Concrete	35.350	0.15	2400

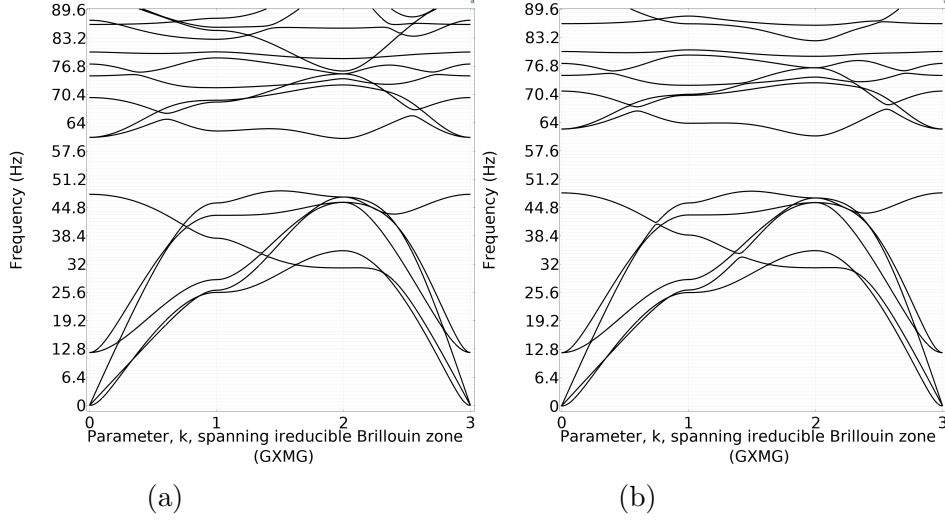


Figure 18: The Floquet-Bloch band diagrams for cylindrical inclusions are obtained around the edges of the irreducible Brillouin zone  $\Gamma XM$ . Note that there is an enhanced bandgap range with twisted 'ligaments' inclusions (a) in comparison to cylindrical inclusion with straight ligaments (b): the bandgap width is approximatively 12 Hz for the former and 15 Hz for the latter, in accordance with earlier study on inertial resonators [56]. Beside that note that a new gap is opening around 80 Hz.